Materials Advances

ROYAL SOCIETY OF CHEMISTRY

PAPER

View Article Online
View Journal | View Issue

Check for updates

Cite this: *Mater. Adv.*, 2022, 3, 8193

Switching endurance of the molecular spin crossover complex $[Fe(HB(tz)_3)_2]$: from single crystals to thin films and electronic devices

Yuteng Zhang,[ab] Lijun Zhang,[a] Karl Ridier,[a] Lionel Salmon,[a] Isabelle Séguy,[b] Gábor Molnár*[a] and Azzedine Bousseksou*[a]

Received 30th June 2022,
Accepted 25th August 2022

DOI: 10.1039/d2ma00802e

rsc.li/materials-advances

The spin-state switching stability of the benchmark $[Fe(HB(tz)_3)_2]$ (tz = 1,2,4-triazol-1-yl) complex is examined in single crystals, thin films and ITO/$[Fe(HB(tz)_3)_2]$/Al metal–insulator–metal junctions. In each case, the switching behavior remains virtually unaltered for more than 10 000 endurance cycles in ambient air, even after more than one-year storage time. The structural/morphological integrity of the samples is not affected to any appreciable extent. On the other hand, the junctions exhibit a slow decrease of their conductance. Based on a comparison with analogous ITO/$[Zn(HB(tz)_3)_2]$/Al junctions, we attribute this phenomenon to the degradation of the device itself, rather than to the deterioration of the SCO properties. These results highlight the intrinsic stability of certain spin crossover compounds, providing impetus for future work, aiming at both the fundamental understanding of this switching stability and its exploitation in technological applications.

Introduction

Several decades ago Olivier Kahn had foreseen the potential integration of molecular spin crossover (SCO) complexes of $3d^4$–$3d^7$ transition metal ions into electronic devices.[1,2] Indeed, SCO compounds exhibit interesting assets for technological applications due to their bistable physical properties (optical, magnetic, electric, *etc.*) and because of the fact that the spin state switching can be triggered by various external stimuli, such as temperature, pressure, light and X-ray irradiation, intense magnetic fields, and the inclusion of solvent/guest molecules.[3–6] These properties along with fast switching speed[7,8] and the versatility of these materials (several hundreds of SCO compounds known) make them appealing for different applications, including information processing, displays, sensors, actuators and so forth.[9]

Notably, several research teams have been working in the past decades to incorporate SCO materials in electronic devices resulting in several remarkable outcomes.[10–17] However, it is fair to admit that we are still at an initial stage in transferring the SCO properties into different device forms and in understanding the relevant physical mechanisms. A particular concern, often evoked regarding molecular materials, is the long-term stability and switching endurance of SCO compounds and SCO-based devices, which is obviously critical for their deployment in any commercially viable technology.[18] Nevertheless, only a few investigations have addressed the robustness of SCO materials, and even less under *in operando* conditions.

The main concern regarding the stability of neat SCO compounds is the large volume change (up to 22%[19]) associated with the spin transition. Depending on the constraints on the sample, this transformational strain leads to the build-up of mechanical stress and, ultimately, to material failure. This inherent mechanical fatigability constitutes a general problem for SCO materials, although not to the same extent, owing to the large structural diversity of SCO complexes (dimensionality, anisotropy, *etc.*). In addition, their switching performance can also be altered by the morphology and microstructure of the sample, environmental factors, in particular by the presence of humidity (or other chemical species), and the switching conditions (speed, homogeneity, *etc.*). In most reported cases, the SCO samples were tested over only a few switching cycles, whose number rarely exceeded 20. Already at this stage, some defects are created and spectacular effects might occur, such as the self-grinding of single crystals reported in ref. 20 and 21. Dedicated endurance tests remain scarce,[22–25] but have been supported recently by the emergence of SCO nanomaterials.[26] Indeed, the most convenient means for inducing the spin-state switching remains thermal excitation, which is a relatively slow process in bulk SCO materials, but can be significantly accelerated at the nanoscale. Capitalizing on this advantage of reduced size scales, Liu *et al.*[25] have

[a] *LCC, CNRS and Université de Toulouse, UPS, INP, F-31077, Toulouse, France. E-mail: gabor.molnar@lcc-toulouse.fr, azzedine.bousseksou@lcc-toulouse.fr*
[b] *LAAS, CNRS and Université de Toulouse, INSA, UPS, F-31077, Toulouse, France*

conducted experiments on Fe-triazole nanoparticles using fast photothermal excitation allowing them to reach 30 000 endurance cycles without any noticeable change of the SCO properties of the nanoparticle. In our group, we have used metallic nanowires for the fast (200 Hz) Joule-heating of thin films of the complex $[Fe(HB(tz)_3)_2]$.[24] Remarkably, the SCO behavior remained virtually the same over more than 10 million spin-state switching events in ambient air. An important open question remains, however, if this robustness is an intrinsic material property or is instead related to the processing of the material as a nanocrystalline film.

Beyond the material level, the degradation of SCO-based electronic devices is further affected by multiple parameters whose impact on device stability remains to be understood. With regard to experience with other types of molecule-based electronic devices, the main factors that influence the stability of the devices are oxygen, humidity, temperature, voltage/current bias and mechanical stress. For instance, oxygen is a well-acknowledged factor that reduces the stability of organic electronic devices. First, metal electrodes (*e.g.* Al) can be oxidized due to oxygen permeation. The metal oxide layer, which exhibits an insulating property, will induce a barrier between the electrode and the active layer, thus influencing the charge injection, which degrades the performance of the device.[26] Second, oxygen molecules may react with the molecules in the active layer resulting in a change of the molecular orbital energy levels and charge carrier mobility of the device.[27] This concern is particularly important for Fe(II)-based SCO molecules, which can be oxidized to Fe(III). The presence of humidity and the application of electrical bias can be co-factors in this context. In addition, oxygen in the active layer will enhance the hole concentration and thereby increase the density of deeper traps for electrons.[28] Besides, heating (working temperature and Joule effect) also plays a vital role in device degradation. Normally, the working temperature is far below the decomposition temperature of the active SCO layer, but it can be a co-factor, which accelerates device degradation.[29]

In the present paper, we report on the investigation of the switching stability of our benchmark SCO compound $[Fe(HB(tz)_3)_2]$ **(1)**. Using similar experimental conditions, we compare the endurance of single crystals, nanometric thin films and thin-film-based metal–insulator–metal resistance switching devices of **(1)**. We show that the outstanding switching resilience of this compound is essentially an intrinsic property, which is only slightly compromised in a device environment, even at relatively long time scales (~year).

Experimental

Samples (crystals, films and electronic junctions) have been prepared using previously published protocols.[30–32] Thermal cycling of the samples has been carried out in ambient air using THMS600, PE120 and HFS350EV-PB4 (Linkam Scientific) heating–cooling stages. The details of the cycles are given in the text. The SCO phenomenon in single crystals and films was detected by measuring their optical transmittance using an Olympus BX51 upright microscope (550 nm) equipped with a CCD camera (Clara, Andor Technology) and a Cary 50 (Agilent) spectrophotometer (318 nm), respectively. The current intensity in the junctions was measured under bias voltages up to 8 V using a Keithley source-meter (model 6430), connected to two gold-tipped tungsten probes. Atomic force microscopy (AFM) surface topography images were acquired under ambient conditions in the tapping mode using a SMART-SPM (Horiba). The grazing incidence X-ray diffraction (GIXRD) patterns of thin films were collected at room temperature using a PANanalytical X'Pert PRO MPD system in a parallel beam configuration using Cu-Kα radiation.

Results and discussion

Transmitted light (550 nm) optical microscopy images of five bulk single crystals, with lateral sizes of a few tens of micrometers, have been recorded during more than 10 000 successive heating and cooling cycles between 58 and 63 °C at a scan rate of 5 °C min^{-1} in ambient air. The optical micrographs provide clear evidence for the well-known abrupt spin transition with hysteresis in **(1)**.[33] Fig. 1 summarizes the main findings for a

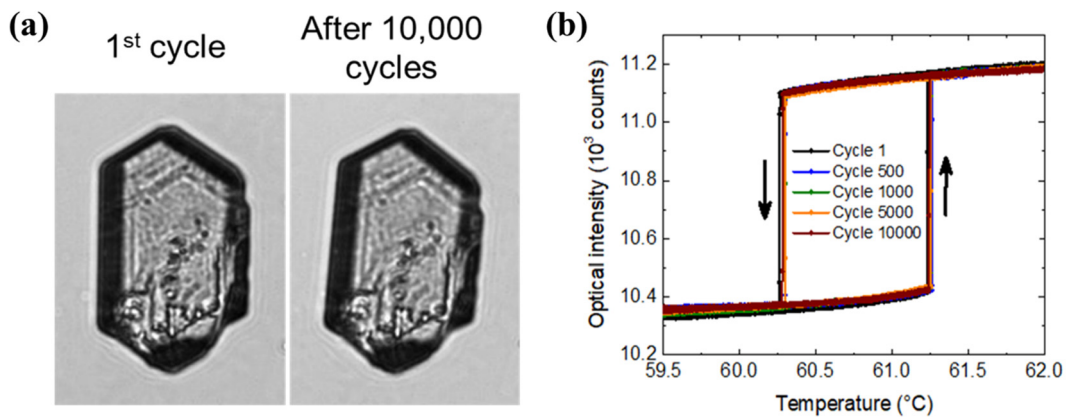

Fig. 1 (a) Optical microscopy images of a single crystal of **(1)** before and after 10 000 spin state switching cycles. (b) Transmitted light intensity through the crystal (550 nm) as a function of the temperature for selected thermal cycles. The heating and cooling processes are shown by arrows.

crystal (53 × 28 × 10 mm^3 size), which has already been extensively investigated five years before,[34] but similar results were obtained for the four other crystals as well. The optical micrographs recorded before cycling and after 10 000 cycles show no obvious change in their morphology (Fig. 1a), revealing that the physical integrity of the crystals has been fully preserved. The spin transition curves recorded for the 1st, 500th, 1000th, 5000th and 10 000th thermal cycles are shown in Fig. 1b. The spin transition is extremely sharp and occurs quasi-isothermally at 61.23 °C and 60.26 °C upon heating and cooling, respectively. During 10 000 thermal cycles, the transition temperatures showed minor, non-monotonous variations, which remain inferior to 0.04 °C. The amplitude of the optical signal variation associated with the SCO phenomenon was less than 4%, which is comparable with the experimental uncertainty.

It is instructive to make a comparison between the cycling behavior of crystals of **(1)** and that of the compound $[Fe(DAPP)(abpt)](ClO_4)_2$ **(2)** (DAPP = bis(3-aminopropyl)(2-pyridylmethyl)amine, abpt = 4-amino-3,5-bis(pyridin-2-yl)-1,2,4-triazole) reported in ref. 20. Whereas crystals of **(1)** remain virtually intact after 10 000 endurance cycles, those of **(2)** are literally pulverized by self-grinding after only 20 thermal cycles. Intriguingly, both compounds are mononuclear and display a similar (*ca.* 4–5%) volumetric strain upon the spin transition. It is tempting to notice, however, that in **(2)** the cohesion of the crystal is maintained by numerous strong intermolecular contacts (π–π stacking and hydrogen-bonds), which are radically reorganized between the high-spin and low-spin forms, whereas the structure of **(1)** exhibits no appreciable strong intermolecular interactions, the cohesion of the lattice instead of arising from numerous weak contacts and dense packing of the molecules. On the other hand, it is important to remark that the SCO properties of **(2)** were not strikingly modified by thermal cycling, the transition became slightly less abrupt and upshifted by *ca.* 5 K after 20 switching events.[20] This contrasts the case of the three-dimensional coordination network $\{Fe(bpe)[Ag(CN)_2]_2\}$ whose crystals were also pulverized after a few switching cycles,

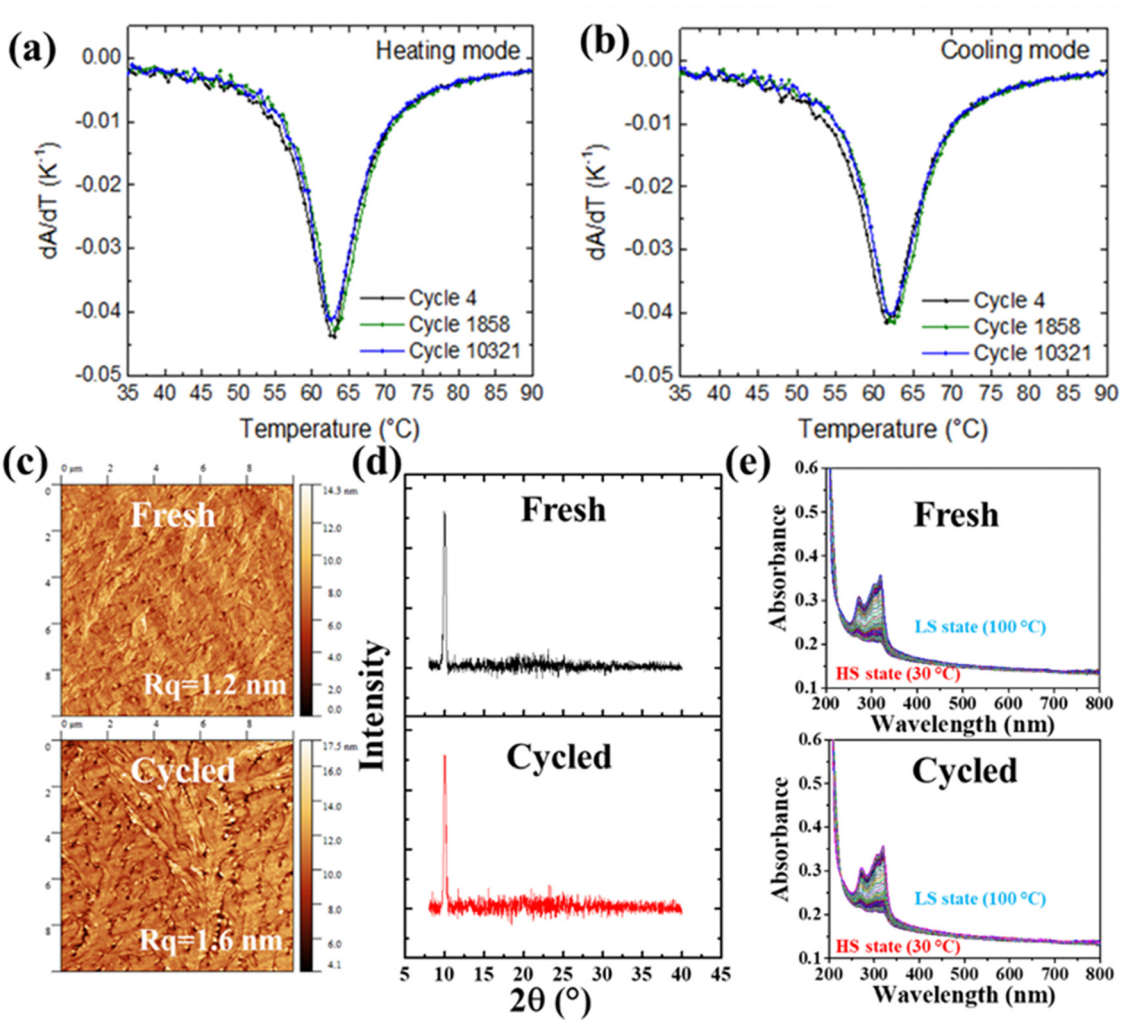

Fig. 2 Top panel: Temperature derivative of the optical absorbance of a 100 nm-thick recrystallized film of **(1)** upon (a) heating and (b) cooling, recorded for selected thermal cycles. Bottom panel: (c) Representative AFM surface topography images. (d) GIXRD patterns and (e) UV-vis spectra of 100 nm-thick films before and after 10 000 thermal cycles.

but this morphological change was accompanied by a drastic alteration of the SCO properties, involving a loss of the initial hysteresis loop and a reduction of the completeness of the transition to *ca.* 50%.[21]

The bulk material (**1**) can be conveniently deposited as an amorphous nanometric film by vacuum thermal evaporation.[31] Annealing of the film in an appropriate solvent vapor (water, acetone, *etc.*) affords for the recrystallization of the film.[35] The cycling stability of a thermally evaporated *ca.* 100 nm thick nanocrystalline film of (**1**) has been analyzed under similar experimental conditions to the crystals (a temperature ramping rate of ±20 °C min^{-1} between 50 and 80 °C). These data, reported previously in ref. 24, are retraced in Fig. 2a and b in the form of temperature derivatives of the optical absorbance of the film. This presentation allows to highlight more clearly the stability of the transition temperatures (represented by the peak positions) and that of the abruptness of the transition curves (represented by the half-height width of the peaks). Overall, the standard deviation of the peak position remains inferior to 0.4 K and the breadth of the transition remains the same within the experimental uncertainty (<1 K). Using an AFM, we have also acquired the surface topography images of a $[Fe(HB(tz)_3)_2]$ film before and after 10 000 thermal cycles to confirm the possible morphological changes. Fig. 2c shows representative topography images revealing the characteristic spherulitic morphology of the films of (**1**).[31] No remarkable change can be observed before and after thermal cycling by visual inspection. The root mean square (RMS) roughness of the selected surface areas remains also the same, with values ranging between 1 and 2 nm. This result contrasts the case of $[Fe(Htrz)_2(trz)](BF_4)$ nanoparticle films,[36] which displayed irreversible changes of the particle morphology (*e.g.* peeling of the surface layers) upon thermal cycling. Fig. 2d and f display the variable temperature UV-vis absorption spectra and GIXRD patterns of new and thermally cycled (>10 000 switches) films. In line with the robust SCO characteristics, these data reveal no appreciable changes of the electronic and crystal structures upon the endurance cycling.

When a nanometric (*ca.* <200 nm) film of (**1**) is embedded in a multilayer ITO/$[Fe(HB(tz)_3)_2]$/Al stack, it forms a

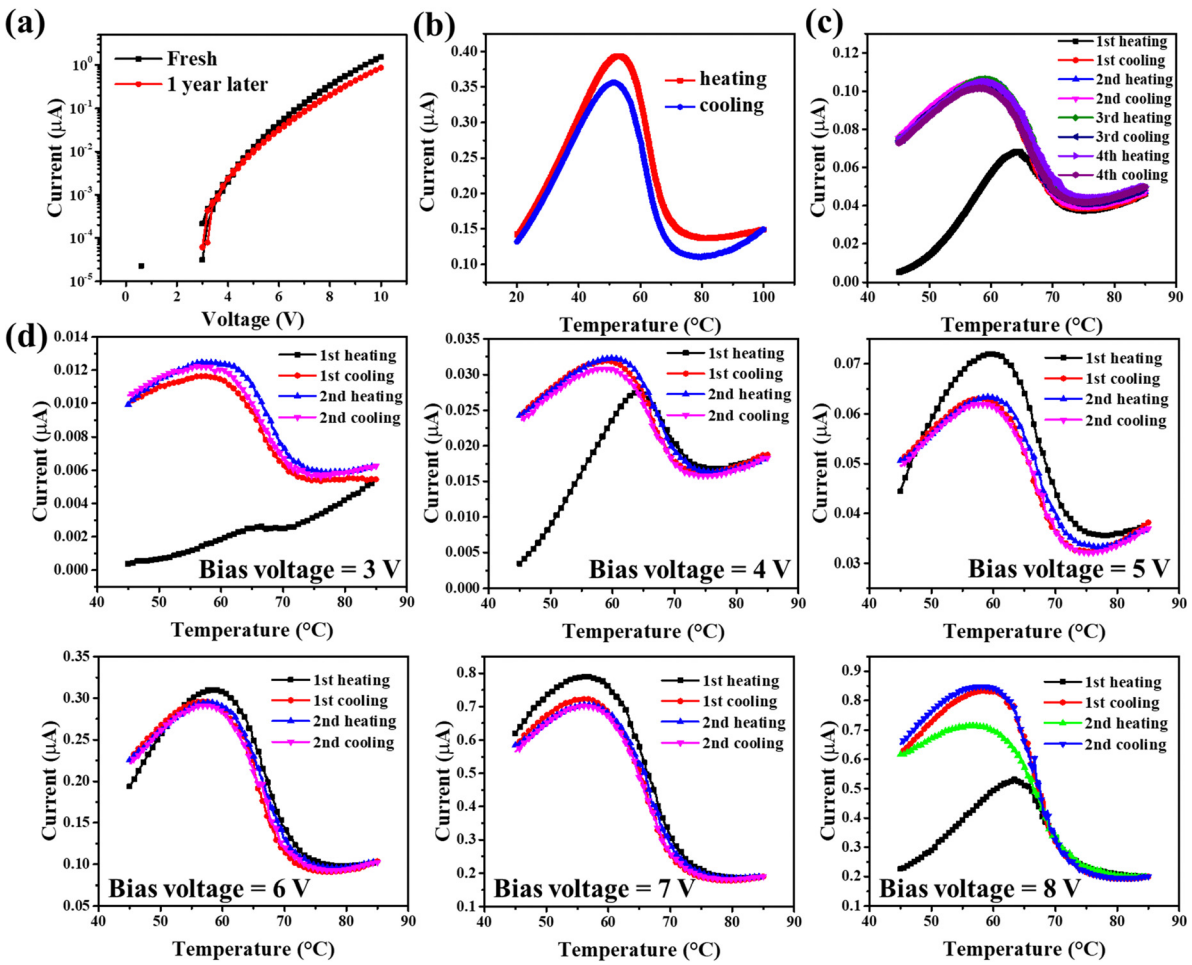

Fig. 3 (a) Room temperature *I*–*V* characteristics of a non-encapsulated ITO/$[Fe(HB(tz)_3)_2]$/Al junction just after fabrication and following 1 year storage under ambient conditions. (b and c) *I*–*T* characteristics of the same junction recorded with an applied bias of 5 V at a scan rate of ±1 °C min^{-1}: (b) as-received (2nd thermal cycle) and (c) 1-year aged. (d) *I*–*T* characteristics of the '1-year-old' junction recorded with different applied bias voltages between 3 and 8 V at a scan rate of ±1 °C min^{-1}. For each applied bias voltage, two successive heating–cooling cycles were carried out.

metal–insulator–metal (MIM) type junction. Previous studies have shown that this type of junctions exhibit an abrupt and reversible decrease of their electrical resistance upon switching the interlayer from the LS to the HS state.[32,37] Depending on the device geometry and experimental conditions, the ON/OFF resistance ratio can vary from a few to a few thousand percent.[37] However, the question of the device stability remained somewhat elusive. With the aim to obtain more insight into this question, we re-examined a non-encapsulated ITO/100 nm $[Fe(HB(tz)_3)_2]$/Al junction, which was left in the ambient laboratory environment (*ca.* 20–25 °C and 50–80% relative humidity) for more than one year. Fig. 3a shows the *I–V* characteristics of the 'as-received' and '1-year-old' junctions. As we can see from this figure, non-encapsulated ITO/SCO/Al preserves reasonably well the initial (non-linear) electrical characteristic of the device after 1 year. The *I–T* characteristics of the same device are shown in Fig. 3b and c for the 'as-received' and '1 year aged' junctions, respectively. In agreement with the *I–V* characteristics, the *I–T* curves confirm the slightly increased resistance of the junction after 1-year storage. More importantly, however, they reveal that the resistance switching properties are maintained in the junction. Indeed, when heating the junction, the spin-state of the Fe(II) ions changes from LS to HS at near 63 °C, which results in an abrupt decrease of the resistance, the HS film being more insulating. The ON/OFF current ratio is *ca.* 3, both in the new and "1-year-old" junctions. Note that we observed a 'run-in' phenomenon in this junction, which can be clearly seen from Fig. 3b (black curve) that the *I–T* characteristics of the first heating are different from all the successive thermal cycles. It is interesting to underline here that this sample was previously heated several times, but after one-year storage, the 'run-in' phenomenon is still perceptible. To further examine this undesired phenomenon, the junction was successively cycled under different applied bias voltages between 3 and 8 V. As shown in Fig. 3d, for each bias voltage, the first heating ramp appears different, whereas the successive cooling–heating cycles are well reproducible. This observation suggests that the reason behind the previously observed irreproducibility of the device performance arises primarily due to the bias ON/OFF switching, whereas the cycling stability is apparently not a major factor. Tentatively, we can ascribe this phenomenon to charge accumulation within the junction when changing the applied bias, which leads to a modified resistance. Upon the first heating, further changes occur *via* charge detrapping, followed by a stationary regime for the successive cycles under a constant bias.

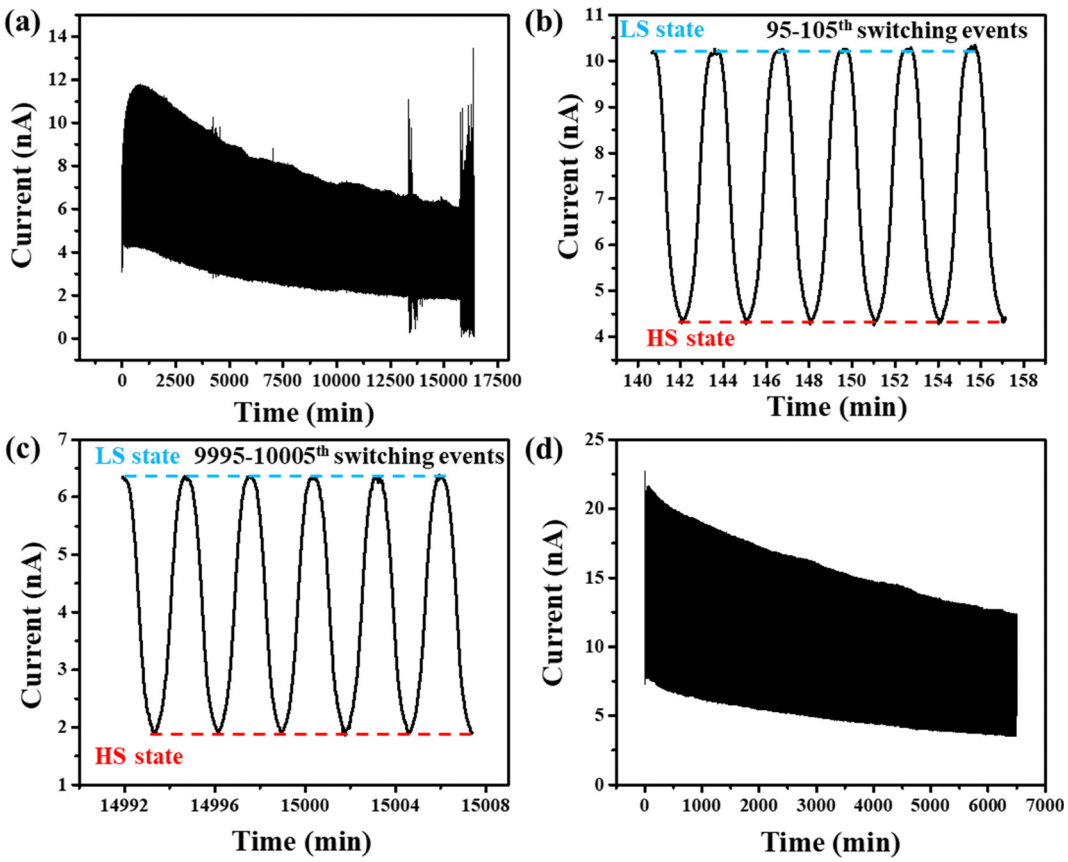

Fig. 4 (a) Current switching cycles between the HS (low current intensity) and LS (high current intensity) states in an ITO/$[Fe(HB(tz)_3)_2]$/Al junction during >10 000 switches under a constant bias voltage of 3 V with a temperature ramping rate of ±20 °C min^{-1} range between 50 and 80 °C. Zooms are also shown for the 95th–105th (b) and the 9995th–10 005th (c) switching events. (d) Current switching cycles in the same junction during >800 switches under a constant bias voltage of 3 V with a temperature ramping rate of ± 5 °C min^{-1} range between 45 and 85 °C.

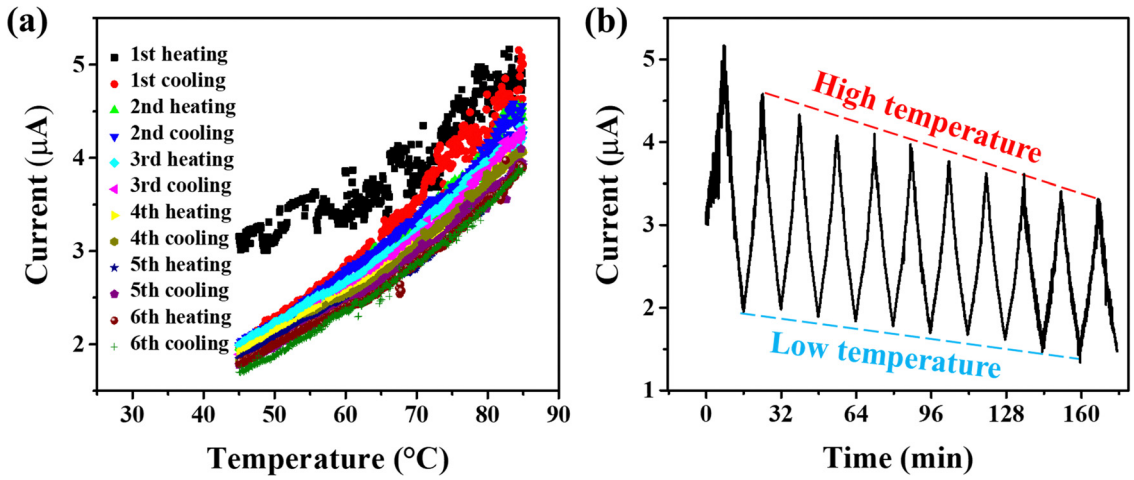

Fig. 5 (a) Successive *I*–*T* cycles in a ITO/[Zn(HB(tz)$_3$)$_2$]/Al junction under a constant bias voltage of 5 V with a temperature ramping rate of ± 5 °C. (b) Variation of the current intensity as a function of the time.

Similar phenomena have been reported in ref. 38 and we believe that this should be a general trend in electronic devices with multiple interfaces and space charge zones.

To obtain a clear-cut picture of the cycling endurance, we then submitted the junction to more than 10 000 thermally induced resistance switching cycles under a constant bias voltage of 3 V with a temperature ramping rate of ±20 °C min^{-1} between 50 and 80 °C. Fig. 4 summarizes the outcome of this non-stop, 12-days-long electrical measurement under ambient conditions (without any protection from the environment). Interestingly, the junction retained the resistance switching properties after such a large number of thermal cycles. Even if the ON/OFF ratio (*ca.* 3) is remarkably stable all along these switching cycles, it is fair to note that the current intensity, which was switched between *ca.* 12 and 4 nA at the beginning of the cycling experiment, is seen to be reduced by a factor two (*i.e.* 6 and 2 nA) after 10 000 thermal cycles. In Fig. 4a, one can note some noise of the current intensity towards the end of the long-time measurement. This phenomenon is most likely related to a slight movement of the measurement tips during the experiment. To remove the doubt that this noise comes from the junction itself, we repositioned properly the probes and we carried out another successive *I*–*T* characterization with a slower temperature ramping rate. These resistance switching cycles are shown in Fig. 4d. As we can see, the junction retained the current switching properties for more than 800 switches and there is no more spurious 'noise' during this measurement.

Despite the remarkable switching endurance of the ITO/[Fe(HB(tz)$_3$)$_2$]/Al junction, the slow and continuous increase of the junction resistance remains an issue. To disentangle the possible contributions to this degradation, we fabricated a similar junction using a film of the isomorphous, complex [Zn(HB(tz)$_3$)$_2$].[39] This compound, which is obviously SCO-inactive, serves us as a comparative system to demonstrate unambiguously any effect linked to the SCO phenomenon. Indeed, as shown in Fig. 5a, the successive *I*–*T* curves of the ITO/[Zn(HB(tz)$_3$)$_2$]/Al junction (non-encapsulated) only display the ordinary thermal activation of the conductivity. Interestingly, the first heating ramp appears spurious for this junction as well, providing support for our hypothesis about the extrinsic origin of this phenomenon (*vide supra*). Another remarkable observation is the monotonous decrease of the current intensity upon thermal cycling, which is illustrated in Fig. 5b. Based on this result, we can thus suggest that the slow increase of the resistance of our MIM junctions is not linked to the spin-state switching phenomenon and it can be thus regarded as a natural 'ageing' of the device, similar to many other organic and molecular electronic devices.

Conclusions

In summary, we have demonstrated that the extremely robust spin-state switching property displayed by the [Fe(HB(tz)$_3$)$_2$] complex is an intrinsic material property, which can be observed both in bulk crystals and nanometric thin films over more than 10 000 endurance cycles in ambient air, even for 'aged' (>year) samples. When the film is integrated into an electronic junction, it preserves its resilience, but the stability of the output signal (current intensity) is compromised to some extent by the inherent fatigability of the device itself. This work shows the possibility to realize long lifetimes and air stable electronic devices using spin crossover complexes. An important open question concerns the structural origin of the robustness of the spin transition in compound [Fe(HB(tz)$_3$)$_2$]. As a working hypothesis, we can evoke the lack of solvent molecules in the structure and the lack of strong interactions, which could interlock the crystal. The latter might therefore exhibit low-barrier solid-state molecular motions (*e.g.* slippage along a specific crystallographic direction) and thus a change of size/shape without breaking under external stimuli. Similar arguments have been put forward in the context of various mechanically responsive, flexible molecular crystals, which may serve as

the source of inspiration.[40–42] From the broader perspective of phase change materials, such as shape memory alloys, the overall crystallographic compatibility of the two phases appears central to achieve high switching endurance.[43,44] Thus, one can expect that neutral, densely packed molecular lattices, wherein the molecules are linked to each other primarily by short-range dispersive forces within isostructural HS and LS lattices, such as in the title compound, are likely to result in advantageous mechanical properties, such as relatively high stiffness and stress resistance. Yet, a deep investigation of the structure–mechanical property relationships *via* experimental and computational methods will be necessary for a better understanding and improved designing of robust SCO materials and devices.

Author contributions

Y. Z.: device fabrication, film and device characterization, data analysis, and writing – original draft; L. Z.: film growth and characterization; K. R.: single crystal characterization; I. S.: supervision, device fabrication and characterization; L. S.: sample fabrication and review; G. M.: supervision and writing – original draft; A. B.: project administration, funding acquisition, conceptualization, and review. The manuscript was read and approved by all named authors.

Conflicts of interest

There are no conflicts to declare.

Acknowledgements

Y. Z. and L. Z. thank the China Scholarship Council for their PhD grant. This work was supported by the LAAS-CNRS micro and nanotechnology platform, a member of the Renatech French national network.

Notes and references

1 O. Kahn, J. Kröber and C. Jay, *Adv. Mater.*, 1992, **4**, 718–728.
2 O. Kahn and C. J. Martinez, *Science*, 1998, **279**, 44–48.
3 P. Gütlich, A. Hauser and H. Spiering, *Angew. Chem., Int. Ed. Engl.*, 1994, **33**, 2024–2054.
4 A. Bousseksou, G. Molnár, L. Salmon and W. Nicolazzi, *Chem. Soc. Rev.*, 2011, **40**, 3313–3335.
5 M. A. Halcrow, ed., *Spin-crossover materials: properties and applications*, John Wiley & Sons, 2013.
6 K. S. Kumar and M. Ruben, *Coord. Chem. Rev.*, 2017, **346**, 176–205.
7 J. K. McCusker, K. N. Walda, R. C. Dunn, J. D. Simon, D. Magde and D. N. Hendrickson, *J. Am. Chem. Soc.*, 1992, **114**, 6919–6920.
8 R. Bertoni, M. Lorenc, H. Cailleau, A. Tissot, J. Laisney, M. L. Boillot, L. Stoleriu, A. Stancu, C. Enachescu and E. Collet, *Nat. Mater.*, 2016, **15**, 606–610.
9 G. Molnár, S. Rat, L. Salmon, W. Nicolazzi and A. Bousseksou, *Adv. Mater.*, 2018, **30**, 1703862.
10 C. Lefter, V. Davesne, L. Salmon, G. Molnár, P. Demont, A. Rotaru and A. Bousseksou, *Magnetochemistry*, 2016, **2**, 18.
11 M. Gruber and R. Berndt, *Magnetochemistry*, 2020, **6**, 35.
12 T. K. Ekanayaka, G. Hao, A. Mosey, A. S. Dale, X. Jiang, A. J. Yost, K. R. Sapkota, G. T. Wang, J. Zhang, A. T. N'Diaye, A. Marshall, R. Cheng, A. Naeemi, X. Xu and P. A. Dowben, *Magnetochemistry*, 2021, **7**, 37.
13 J. Dugay, M. Aarts, M. Giménez-Marqués, T. Kozlova, H. W. Zandbergen, E. Coronado and H. S. J. van der Zant, *Nano Lett.*, 2017, **17**(1), 186–193.
14 N. Konstantinov, A. Tauzin, U. Nguetchuissi Noumbé, D. Dragoe, B. Kundys, H. Majjad, A. Brosseau, M. Lenertz, A. Singh, S. Berciaud, M. L. Boillot, B. Doudin, T. Mallah and J.-F. Dayen, *J. Mater. Chem. C*, 2021, **9**, 2712–2720.
15 L. Poggini, M. Gonidec, J. H. Gonzalez-Estefan, G. Pecastaings, B. Gobaut and P. Rosa, *Adv. Electron. Mater.*, 2018, **4**, 1800204.
16 F. Prins, M. Monrabal-Capilla, E. A. Osorio, E. Coronado and H. S. van der Zant, *Adv. Mater.*, 2011, **23**, 1545–1549.
17 S. K. Karuppannan, A. Martín-Rodríguez, E. Ruiz, P. Harding, D. J. Harding, X. Yu, A. Tadich, B. Cowie, D. Qi and C. A. Nijhuis, *Chem. Sci.*, 2021, **12**, 2381–2388.
18 J. Zarembowitch, F. Varret, A. Hauser, J. A. Real and K. Boukheddaden, *C. R. Chim.*, 2018, **21**, 1056–1059.
19 M. Grzywa, R. Röß-Ohlenroth, C. Muschielok, H. Oberhofer, A. Błachowski, J. Żukrowski, D. Vieweg, H.-A. K. Von Nidda and D. Volkmer, *Inorg. Chem.*, 2020, **59**, 10501–10511.
20 Y. Miyazaki, T. Nakamoto, S. Ikeuchi, K. Saito, A. Inaba, M. Sorai, T. Tojo, T. Atake, G. S. Matouzenko, S. Zein and S. A. Borshch, *J. Phys. Chem. B*, 2007, **111**, 12508–12517.
21 J. A. Real, A. B. Gaspar and M. C. Munoz, *Dalton Trans.*, 2005, 2062–2079.
22 C. Lefter, R. Tan, S. Tricard, J. Dugay, G. Molnár, L. Salmon, J. Carrey, A. Rotaru and A. Bousseksou, *Polyhedron*, 2015, **102**, 434–440.
23 M. Piedrahita-Bello, J. E. Angulo-Cervera, A. Enriquez-Cabrera, G. Molnár, B. Tondu, L. Salmon and A. Bousseksou, *Mater. Horiz.*, 2021, **8**, 3055–3062.
24 K. Ridier, A.-C. Bas, Y. Zhang, L. Routaboul, L. Salmon, G. Molnár, C. Bergaud and A. Bousseksou, *Nat. Commun.*, 2020, **11**, 1–9.
25 S. Liu, K. Zhou, T. Yuan, W. Lei, H.-Y. Chen, X. Wang and W. Wang, *J. Am. Chem. Soc.*, 2020, **142**, 15852–15859.
26 M. Glatthaar, M. Riede, N. Keegan, K. Sylvester-Hvid, B. Zimmermann, M. Niggemann, A. Hinsch and A. Gombert, *Sol. Energy Mater. Sol. Cells*, 2007, **91**, 390–393.
27 M. O. Reese, A. M. Nardes, B. L. Rupert, R. E. Larsen, D. C. Olson, M. T. Lloyd, S. E. Shaheen, D. S. Ginley, G. Rumbles and N. Kopidakis, *Adv. Funct. Mater.*, 2010, **20**, 3476–3483.
28 J. Schafferhans, A. Baumann, A. Wagenpfahl, C. Deibel and V. Dyakonov, *Org. Electron.*, 2010, **11**, 1693–1700.
29 X. Zhan, Z. A. Tan, B. Domercq, Z. An, X. Zhang, S. Barlow, Y. Li, D. Zhu, B. Kippelen and S. R. Marder, *J. Am. Chem. Soc.*, 2007, **129**, 7246–7247.
30 S. Rat, K. Ridier, L. Vendier, G. Molnár, L. Salmon and A. Bousseksou, *CrystEngComm*, 2017, **19**, 3271–3280.

31 V. Shalabaeva, S. Rat, M. D. Manrique-Juarez, A.-C. Bas, L. Vendier, L. Salmon, G. Molnár and A. Bousseksou, *J. Mater. Chem. C*, 2017, **5**, 4419–4425.
32 V. Shalabaeva, K. Ridier, S. Rat, M. D. Manrique-Juarez, L. Salmon, I. Séguy, A. Rotaru, G. Molnár and A. Bousseksou, *Appl. Phys. Lett.*, 2018, **112**, 013301.
33 K. Ridier, S. Rat, H. J. Shepherd, L. Salmon, W. Nicolazzi, G. Molnár and A. Bousseksou, *Phys. Rev. B*, 2017, **96**, 134106.
34 K. Ridier, S. Rat, L. Salmon, W. Nicolazzi, G. Molnár and A. Bousseksou, *Phys. Chem. Chem. Phys.*, 2018, **20**, 9139–9145.
35 A. C. Bas, V. Shalabaeva, X. Thompson, L. Vendier, L. Salmon, C. Thibault, G. Molnár, L. Routaboul and A. Bousseksou, *C. R. Chim.*, 2019, **22**, 525–533.
36 M. D. Manrique-Juárez, I. Suleimanov, E. M. Hernández, L. Salmon, G. Molnár and A. Bousseksou, *Materials*, 2016, **9**, 537.
37 Y. Zhang, I. Séguy, K. Ridier, V. Shalabaeva, M. Piedrahita-Bello, A. Rotaru, L. Salmon, G. Molnár and A. Bousseksou, *J. Phys.: Condens. Matter*, 2020, **32**, 214010.
38 E. P. van Geest, K. Shakouri, W. Fu, V. Robert, V. Tudor, S. Bonnet and G. F. Schneider, *Adv. Mater.*, 2020, **32**, 1903575.
39 K. Ridier, Y. Zhang, M. Piedrahita-Bello, C. M. Quintero, L. Salmon, G. Molnar, C. Bergaud and A. Bousseksou, *Adv. Mater.*, 2020, **32**, 2000987.
40 A. Hasija and D. Chopra, *CrystEngComm*, 2021, **23**, 5711–5730.
41 P. Naumov, S. Chizhik, M. K. Panda, N. K. Nath and E. Boldyreva, *Chem. Rev.*, 2015, **115**, 12440–12490.
42 C. M. Reddy, G. R. Krishna and S. Ghosh, *CrystEngComm*, 2010, **12**, 2296–2314.
43 C. Chluba, W. Ge, R. Lima de Miranda, J. Strobel, L. Kienle, E. Quandt and M. Wuttig, *Science*, 2015, **348**, 1004–1007.
44 D. Lee, B. Chung, Y. Shi, G.-Y. Kim, N. Campbell, F. Xue, K. Song, S.-Y. Choi, J. P. Podkaminer, T. H. Kim, P. J. Ryan, J.-W. Kim, T. R. Paudel, J.-H. Kang, J. W. Spinuzzi, D. A. Tenne, E. Y. Tsymbal, M. S. Rzchowski, L. Q. Chen, J. Lee and C. B. Eom, *Science*, 2018, **362**, 1037–1040.